Coupled Temperature and Tracer Data Analysis Using a Uniform Porous Channel Model

Carla Kathryn D. Co and Roland N. Horne

Department of Energy Resources Engineering, Stanford University, Stanford, CA, USA

Keywords

Geothermal, tracer breakthrough, connectivity, thermal response, production, injection, porous model

ABSTRACT

Characterization of permeable zones is of primary importance for geothermal reservoir management. Spent brine is routinely injected in geothermal systems for pressure support and waste water disposal. Therefore, producer and injector interwell connectivity derived from feedzone characterization will influence the mass and heat transport of the injected fluid. Several model configurations are available in the literature to describe these connections. Analytical models for heat and tracer mass transport related to the uniform porous channel configuration are described in this study. Both tracer and temperature data are used for calibration to constrain the multiple degrees of freedom.

Levenberg-Marquardt and Trust-Region-Reflective nonlinear least squares algorithms were applied to determine the optimized parameter values. Calculated parameters included the following: channel width, channel height, porosity, pore diffusivity, and equivalent injection temperature in the channel. Normalized tracer and thermal response datasets from injector-producer well pairs from Hijiori and Palinpinon fields were used for calibration. Results showed a good fit between the analytical models and the measured data points. Wells NJ2RD and NJ5D from the Palinpinon field exhibited the strongest interwell connectivity and highest diffusivity coefficient among the three well pairs. The two Palinpinon field well pairs showed significant mixing with hotter fluids prior to injection which was expected in a conventional hydrothermal reservoir. On the other hand, the well pair HDR1-HDR3 in Hijiori had the lowest diffusivity coefficient and equivalent injection temperature because it was in an EGS reservoir. Combined thermal and tracer data analyses yielded a detailed characterization of interwell connectivity. It was recommended that this method be applied to other models configurations to compare the range of thermal response to injection.

1. Introduction

Injection of spent brine and condensate is practiced widely in geothermal fields for pressure support and wastewater disposal (Horne, 1996). However, premature thermal breakthrough can occur if injection is not managed properly. Therefore, determination of interwell connectivity is important for proper reservoir management. Connectivity between production and injection wells can be represented by different permeable zone configurations with their corresponding tracer and heat transport analytical models. Figure 1a describes a single fracture connection model (Co and Horne, 2011; Horne, 1996). In this configuration, the fracture aperture is the most significant geometric parameter affecting transport properties. The second model (Figure 1b) uses a well-developed major fault with an impermeable core and permeable damage zones (Massart et al., 2010; Paul et al., 2009, Paul et al., 2011; Johri et al., 2012). A third model, shown in Figure 1c, utilizes sheared fracture planes or porous channels (Bullivant and O'Sullivan, 1985; Lauwerier, 1955; Gringarten and Sauty, 1975) that can be attributed to secondary structures subparallel to major

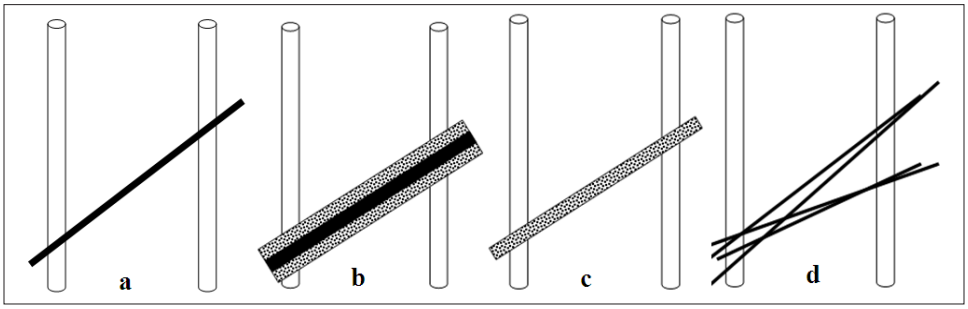

Figure 1. Interwell connectivity configurations: (a) single fracture connection; (b) well-developed fault with damage zones and a low permeability core; (c) secondary structures subparallel to faults or stratigraphy based connections; (d) cross-cutting sheared fracture planes.

faults. In addition, horizontal sheared fracture planes can be used to model lithological boundaries that are often idealized as brecciated zones. Lastly, the fourth model (Figure 1d) describes the intersection of cross-cutting sheared fracture planes as possible geothermal permeable zones. These could be represented by parallel plate models (Gringarten et al., 1975, Rivera et al., 1987).

Several attempts have been made in the past to describe channel geometry by matching tracer test data, mostly without success. This was because the parameter estimation problem had multiple degrees of freedom, which made it difficult to separate the channel width from other unknown reservoir parameters. Thermal response data could be used to constrain the degrees of freedom. Co and Horne (2011) proposed a single fracture model to describe the connectivity of an injection and production well pair. Fracture aperture or width was estimated using tracer and thermal data for this simplified model. This study aimed to describe interwell connections through characterization of permeable zones in geothermal wells using a coupled analysis of both tracer and thermal response datasets. A porous or brecciated channel model configuration was described and investigated.

Tracer returns and temperature responses were obtained from available literature data. Analytical models for tracer transport and reservoir cooling were derived, as will be described in the next section. Unknown parameters affecting these were determined using nonlinear least squares methods on normalized or scaled tracer and thermal response data points. Of particular importance for this permeable zone configuration was the channel half aperture (b), which influences the mass and heat transport through EGS and conventional or hydrothermal reservoirs. The total volume contacted, or the product of geometric parameters, reflected the degree of connectivity of the well pairs. Based on the results, conclusions and recommendations on the application of this method were made.

2. Analytical Models

Tracer Transport

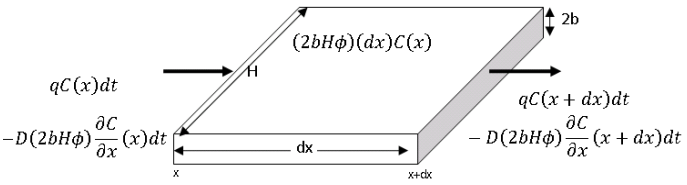

Figure 2. Impulse tracer mass transport derivation schematic: the injection well is on the left while the production well is on the right.

Figure 2 describes the schematic for the impulse tracer injection case with advection and longitudinal diffusion in the x-direction. Here, the x-direction is the flow path of the tracer from the injector on the left side to the producer on the right. The half aperture, b, is an important fracture plane parameter that can be determined from borehole imaging data. For well-developed and large-scale sealing faults, the effective total aperture is the half width of the damage zone. This is because the opposite sides of the fault are noncommunicating. D is the longitudinal diffusion coefficient, while H and ϕ are the fracture plane height and porosity, respectively. The governing advection-dispersion equation for this porous system is shown in Equation 1, where v is the pore velocity of the injected fluid. Using the impulse boundary condition on the left side and a semi-infinite plane boundary in the x-axis, the well-known solution of tracer concentration dependency on distance (x) and time (t) can be derived (Equation 2). This solution has also been derived in previous studies (Bullivant and O'Sullivan, 1985; Kreft and Zuber, 1978). Another form of Equation 2 can be derived in terms of the Peclet number (w), which is the dimensionless ratio of the advection and diffusion terms; as well as the mean tracer arrival time (t_m) (Equation 3). Definitions of these two parameters are shown in Equations 4 and 5 with volumetric injection rate (q), the cross-sectional area (A), and porosity (ϕ). For tracer analysis alone, the Peclet number and mean tracer arrival time are used to obtain a match for Equation 3. This implies that the parameters are lumped together, which makes it difficult to isolate individual values. Hence, coupling the tracer and temperature data analyses will yield a better match by constraining the possible geometric configurations and providing more data calibration points. This can then be used to generate more reliable temperature response predictions for different injection schemes.

$$D\frac{\partial^2 C}{\partial x^2} - v\frac{\partial C}{\partial x} = \frac{\partial C}{\partial t} \tag{1}$$

$$C(x,t) = \frac{m\phi}{q}\frac{1}{2}\frac{x}{\sqrt{D}}\frac{1}{\sqrt{\pi t^3}}\left[e^{\frac{-(x-vt)^2}{4Dt}}\right] \tag{2}$$

$$C(x,t) = \frac{m\phi}{2q}\sqrt{\frac{t_m w}{\pi}}\frac{1}{t^{1.5}}\ exp\left\{-\frac{w}{4}\frac{(t-t_m)^2}{tt_m}\right\} \tag{3}$$

$$t_m = \frac{\phi x A}{q} \tag{4}$$

$$w = \frac{qx}{vA} = \frac{qx}{D\phi A} \tag{5}$$

Heat Transport

Several studies have modeled the temperature drawdown caused by constant cold water injection into a porous and permeable channel in hot geothermal systems (Lauwerier, 1955; Gringarten and Sauty, 1975). Schematic diagrams for the heat flow streams for the permeable fluid saturated rock and impermeable rock matrix are shown in Figures 3 and 4, respectively. The temperature of the low permeability matrix or host rock is (T_r) and the temperature of the fluid saturated rock is (T_w). Specific heat capacities (by mass) for the fluid saturated rock and water are c_A and c_w, respectively. Densities of the fluid saturated rock and water are ρ_r and ρ_w such that ($\rho_A c_A$) is the saturated rock specific heat capacity by volume as defined in Equation 6. K_r is the rock thermal conductivity and the other variables related to geometry have the same definition as described in the tracer transport section.

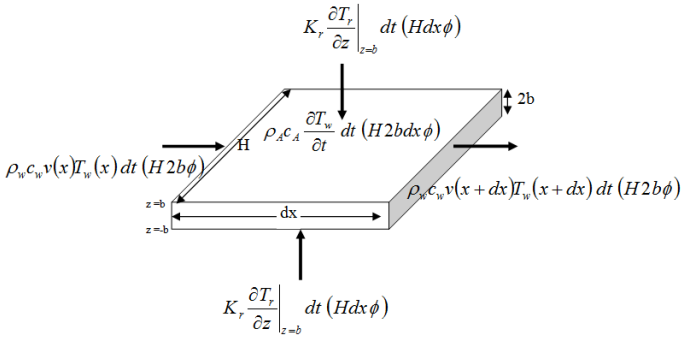

Figure 3. Constant injection heat transport derivation schematic for the fluid saturated rock: the injection well is on the left while the production well is on the right.

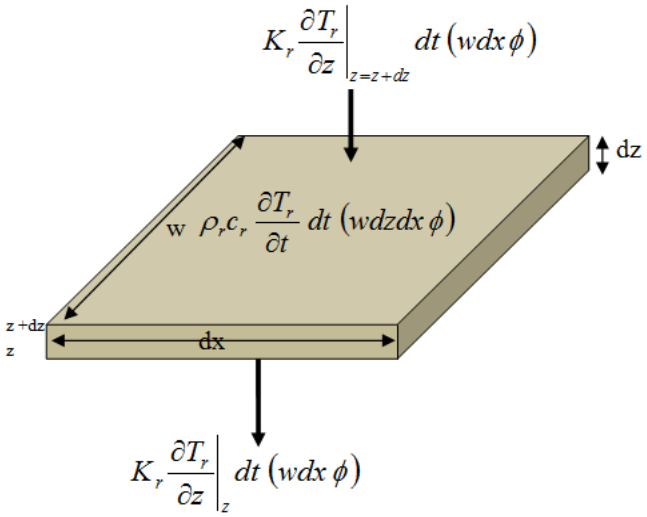

Figure 4. Constant injection heat transport derivation schematic for the impermeable rock matrix: there are two of these along the z-direction conducting heat to the fluid saturated rock in Figure 3.

Heat is transported by the convection within the porous zone in the x-direction and conduction from the rock matrix to this permeable zone in the z-direction. One important assumption of this model is the instantaneous thermal equilibrium between the rock matrix and the fluid saturated rock. Another assumption is that the rock and fluid properties are constant. From the energy balance of all the heat streams, the partial differential equations for the permeable zone (Equation 7) and the impermeable rock matrix (Equation 8) can be derived. The first boundary condition is instantaneous thermal equilibrium and the second boundary condition is constant injection temperature on the left side. Initial conditions for these systems are the same initial temperature for the rock matrix and saturated rock (T_o) as well as the constant injection temperature on the left ($T_{injection}$). Using iterative Laplace transform, the solution to these two partial differential equations can be derived as shown in Equation 9. Typically, the temperature drawdown at the producer is defined in terms of the temperature ratio (T_{ratio}) of the resulting temperature decrease due to injection ($T_w - T_o$) and the difference between the injection and initial temperatures ($T_{injection} - T_o$). In the next section, the optimization methodology will be described in more detail.

$$\rho_A c_A = \phi\rho_w c_w + (1-\phi)\rho_r c_r \tag{6}$$

$$K_r \left.\frac{\partial T_r}{\partial z}\right|_{z=b} = b\rho_A c_A \frac{\partial T_w}{\partial t} + b\rho_w c_w v \frac{\partial T_w}{\partial x} \quad for\ |z| \le b \tag{7}$$

$$K_r \frac{\partial^2 T_r}{\partial z^2} = \rho_r c_r \frac{\partial T_r}{\partial t} \quad for\ |z| > b \tag{8}$$

$$T_{ratio}(x,t) = \frac{T_w(x,t) - T_o}{T_{injection} - T_o} = erfc \frac{\frac{1}{b}\sqrt{\frac{K_r}{\rho_w c_w v}}x}{2\sqrt{\frac{\rho_A c_A}{\rho_r c_r}\left(\frac{\rho_w c_w v}{\rho_A c_A}t - x\right)}} \tag{9}$$

3. Methodology

In order to couple both the tracer returns concentration and temperature responses for the analytical models, they were scaled to have the same order of magnitude. This was to ensure that both tracer and temperature responses would be given equal weights in the optimization. Scaling was done by using the normalized concentration ($\bar{C}$) and temperature ($\bar{T}$) data vectors as described in Equations 10 and 11, respectively. Here, the maximum and minimum subscripts referred to the maximum and minimum values for the tracer concentration and temperature datasets. Thus, both normalized data vectors had values that ranged from 0 to 1. The same scaling was done with the calculated values of the model.

Nonlinear least squares optimization was used to determine the relevant geometric and fluid flow parameters defined as the y vector in Equation 12. Parameters included were: channel half width (b), channel height (H), channel porosity (ϕ), saturated rock pore diffusivity (D), and equivalent injection temperature in the porous channel ($T_{injection}$). The total residual error vector, $\bar{F}(\bar{y})$, was a combination of the error vectors for the normalized concentration and temperature as shown in Equation 13. Error was defined as the absolute difference between the calculated values from the model and the measured data points. Using the square of the 2-norm of the vector $\bar{F}$ as the objective function (f), nonlinear least squares optimization was used to determine the parameter vector ($\bar{y}$) that minimized f as defined by Equation 14. Levenberg-Marquardt and Trust-Region-Reflective algorithms were applied. These minimized the objective function that was bounded. A first order optimality measure was used as the stopping criterion (Equation 15). Iterations were done until the change in value of the objective function during an iteration step ($n + 1$) was less than 10^{-10}. This method was applied to field data as will be described in the next section.

$$\bar{C} = \frac{\bar{C}}{C_{maximum}} \tag{10}$$

$$\bar{T} = \frac{\bar{T} - T_{minimum}}{T_{maximum} - T_{minimum}} \tag{11}$$

$$\vec{y} = \begin{bmatrix} b & H & \phi & D & T_{injection} \end{bmatrix} \quad (12)$$

$$\vec{F}(\vec{y}) = \left\{ \left| \overline{C}_{calc}(\vec{y}) - \overline{C}_{data} \right| \quad , \quad \left| \overline{T}_{calc}(\vec{y}) - \overline{T}_{data} \right| \right\} \quad (13)$$

$$\min_{\vec{y}} f = \min_{\vec{y}} \left\| \vec{F}\left(\vec{y}\right)_2^2 \right\| = \min_{\vec{y}} \sum_k F_k^2\left(\vec{y}\right) \quad (14)$$

$$\left| f\left(\vec{y}_n\right) - f\left(\vec{y}_{n+1}\right) \right| < 10^{-10} \quad (15)$$

4. Application to Field Data

Table 1 lists the injection and production well pairs with tracer and temperature data available in published literature. All were used in this study. Hijiori is an EGS field while Palinpinon is a conventional liquid-dominated reservoir. Tracers test results are often readily available in literature, however thermal breakthrough data are infrequent. In Hijiori, temperature data were derived from long-term circulation tests (Matsunaga et al., 2002; Matsunaga et al., 2005). Reservoir temperatures for the Palinpinon field were reported by Maturgo et al. (2010). Rock and fluid thermal transport properties and fluid densities are assumed to be constant with values from Table 2.

Table 1. Injection-production well pairs analyzed.

Field	Injector	Producer	Source
Hijiori	HDR-1	HDR-3	Matsunaga et al. (2002) Matsunaga et al. (2005)
Palinpinon	NJ2RD	NJ5D	Maturgo et al. (2010)
	SG2RD	NJ3D	

Table 2. Assumptions used in calculations.

Rock thermal conductivity	K_r	2	W/m-C
Rock density	ρ_r	2200	kg/m^3
Water density	ρ_w	1000	kg/m^3
Rock heat capacity	C_r	0.712	kJ/kg-C
Water heat capacity	C_w	4.342	kJ/kg-C

Results from the optimization are shown in Table 3. Channel geometry related parameters are the following: half aperture (b), height (H), and porosity (ϕ). Saturated pore diffusivity (D) and equivalent channel injection temperature ($T_{injection}$) are related to transport. As described in previous sections, the equivalent injection temperature takes into account the mixing of the injected fluid with other feed zones. Because it is an EGS reservoir, the Hijiori well pair (HDR-1 and HDR-3) is expected to have a lower injection temperature as calculated. Both Palinpinon field well pairs have high $T_{injection}$ values because they are from a conventional geothermal reservoir, where there are multiple high enthalpy feed zones expected. In terms of pore diffusivity, the Hijiori well pair value is smaller by an order of magnitude compared to the other two at 0.01 m^2/s. This can be attributed as well to the nature of the EGS reservoir, where a few flow paths are present and advective transport dominates. In contrast, relative values of porosities and channel heights are similar for the three well pairs. Porosity values range from 0.15 to 0.19, which is consistent with either secondary damage zone or brecciated zone models. Channel half aperture values for HDR1-HDR-3 and SG2RD-NJ3D well pairs have the same order of magnitude. On the other hand, NJ2RD-NJ5D has the largest half aperture at 5.64m. This well pair likewise has the largest pore diffusivity of 0.230 m^2/s. Therefore, one can conclude that this well pair has the greatest connectivity among the three. Table 4 shows the parameters derived by Maturgo et al. (2010) from tracer analysis of the same Palinpinon field data. There is significant difference for all the parameters when compared to those derived from the nonlinear least squares optimization. Because it is based solely on tracer analysis, one would not be able to match the thermal response using these values. This illustrates the importance of constraining the possible configurations of the porous model.

Table 3. Geometric and fluid flow parameters derived from the analytical models.

Injector	Producer	b m	H m	ϕ	D m^2/s	$T_{injection}$ C
HDR-1	HDR-3	0.73	1246	0.23	0.010	100
NJ2RD	NJ5D	5.64	1296	0.15	0.230	236
SG2RD	NJ3D	0.51	1127	0.19	0.138	259

Table 4. Geometric and fluid flow parameters from tracer analysis (Maturgo et al.,2010).

Injector	Producer	b m	H m	ϕ	$T_{injection}$ C
NJ2RD	NJ5D	2.44	104	0.10	160
SG2RD	NJ3D	2.18	91	0.10	160

Figure 5 shows the normalized tracer response (C_{ratio}) curve fit versus time using the parameters described in Table 3 for the HDR-1 and HDR-3 well pair. The tracer response curve is flat with no sharp peaks. On the other hand, Figure 6 shows the thermal response curve fit. Red crosses are the measured data points while the blue line represents the optimized curve. Overall, a good match can be observed. However, because all the data points are honored by the optimization, outliers force the match towards the middle of all the data. This is more pronounced in the temperature data because they are generally more scattered. The same phenomenon can be observed for the normalized tracer concentration (Figure 7) and temperature response (Figure 8) curve fit for the NJ2RD-NJ5D well pair. For this case, the typical single peak tracer returns behavior with a tail can be observed. Aside from meeting the objective function tolerance per step, the tracer return curve fit should match the peak concentration time effectively. Measured thermal response data for this well pair are also slightly scattered but a sufficient match is obtained. Similarly, a standard tracer return profile can be noticed for the SG2RD-NJ3D well pair (Figure 9). The resulting model matches this extremely well. Equivalent thermal response curve fit is shown in Figure 10. There is significant scattering of measured data but the model still matches them adequately.

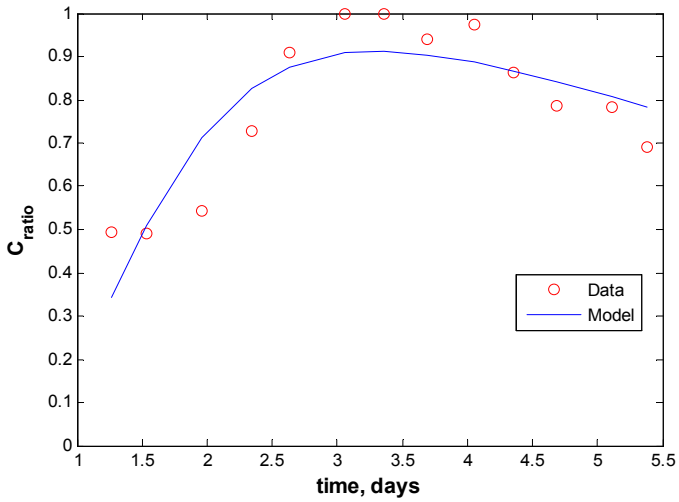

Figure 5. Normalized tracer response curve fit for HDR1(Injector)-HDR3(Producer). Measured data points are in red crosses while the analytical model result is represented by the blue line.

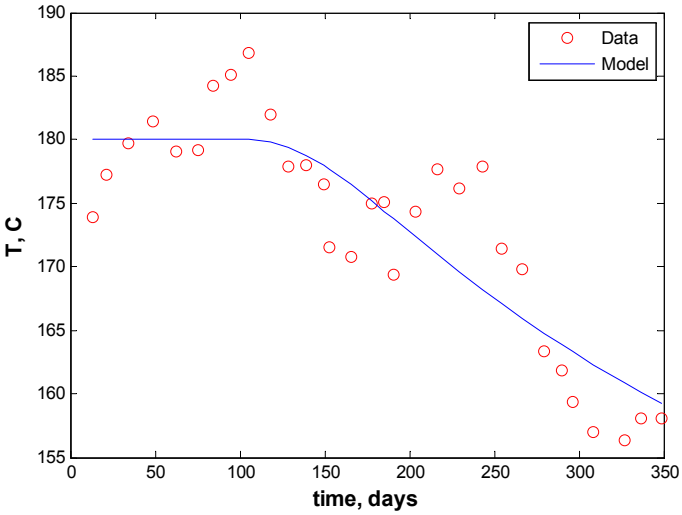

Figure 6. Thermal response curve fit for HDR1(Injector)-HDR3(Producer).

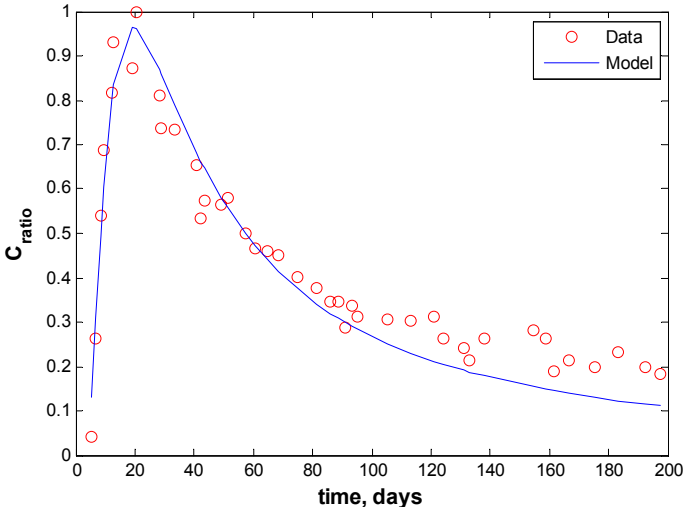

Figure 7. Normalized tracer response curve fit for NJ2RD(Injector)-NJ5D(Producer).

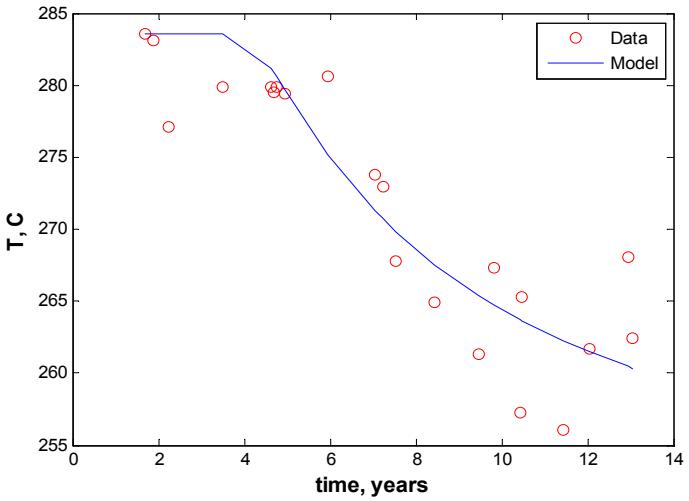

Figure 8. Thermal response curve fit for NJ2RD(Injector)-NJ5D(Producer).

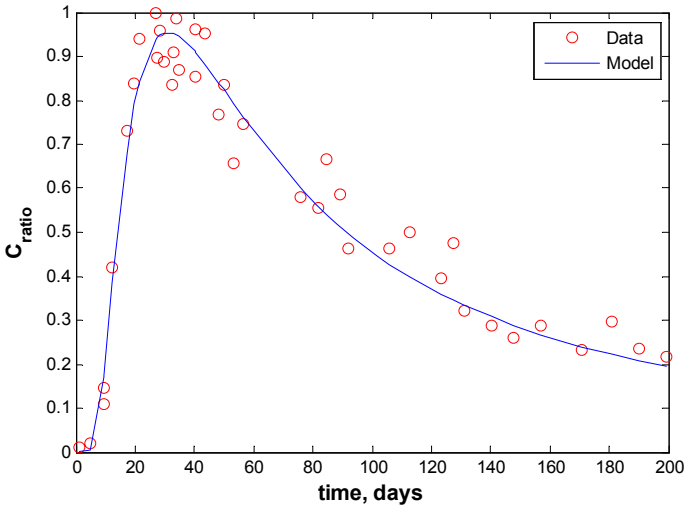

Figure 9. Normalized tracer response curve fit for SG2RD(Injector)-NJ3D(Producer).

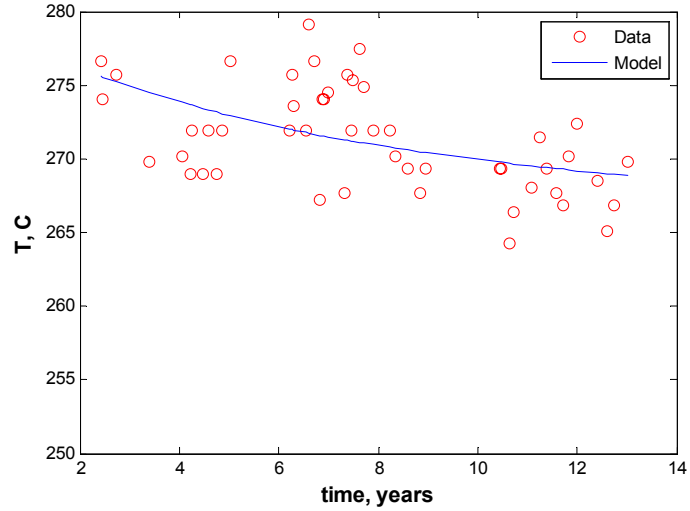

Figure 10. Thermal response curve fit for SG2RD(Injector)-NJ3D(Producer).

5. Conclusions

Producer and injector interwell connectivity derived from feedzone characterization will influence the mass and heat transport of the injected fluid. Moreover, characterization of the interwell connectivity would aid in the prevention of premature thermal breakthrough from injection wells through proper reservoir management. Several idealized model configurations of interwell connectivity are available. The uniform porous channel model can be used to represent secondary damage zones or brecciated regions as permeable zones. A combination of thermal and tracer response analyses for this model can be used to determine unknown reservoir and fluid parameters using nonlinear least squares optimization. The total channel volume represents the strength of connectivity of a well pair. Meanwhile, the channel half width or aperture describes the degree of heat transfer from the matrix to the porous channel. Pore diffusivity is an indication of the amount of dispersion or diffusion within the channel. Lastly, the equivalent injection temperature at the channel models the amount of fluid mixing with other permeable zones.

Among the three well pairs investigated in this study, NJ2RD-NJ5D from the Palinpinon field exhibited the strongest interwell connectivity. This pair also had the highest diffusivity coefficient and channel width. Generally, well pairs from conventional hydrothermal reservoirs showed significant mixing with hotter fluids prior to injection. In contrast, the EGS well pair from Hijiori (HDR1-HDR3) had the lowest diffusivity coefficient and equivalent injection temperature. This is expected due to the limited number of flow paths in this type of reservoir.

Overall, the coupling of thermal and tracer response analyses results in the detailed characterization of interwell connectivity which could be used to predict future thermal response to injection. It is recommended that this combined analysis method be used for other model configurations as well. Furthermore, cooling predictions from these different models could be compared to obtain the range of possible thermal response outcomes from injection.

6. Acknowledgements

The authors acknowledge the support of the Department of Energy (under contract number DE-FG36-08GO18192).

7. References

Bayon, F.E.B. and Ogena, M.S.: "Handling the Problem of Rapid Reinjection Returns in Palinpinon-I and Tongonan, Philippines," *Proceedings,* World Geothermal Congress. 2005.

Bullivant, D.P. and O'Sullivan, M.J.: "Some simple models of tracer tests," *Proceedings*, 7th New Zealand Geothermal Workshop. 1985.

Co, C.K.D. and Horne, R.N.: "Characterization of Geothermal Interwell Connectivity Using Thermal and Tracer Data," *GRC Transactions*. 2011, 1411-1416.

Gringarten, A.C., and Sauty, J. P.: "A theoretical study of heat extraction from aquifers with uniform regional flow," *Journal of Geophysical Research*, 80(35). 1975, 4956-4962.

Gringarten, A.C., Witherspoon, P.A., and Ohnishi, Y.: "Theory of heat extraction from fractured hot dry rock," *Journal of Geophysical Research*, 80(8). 1975, 1120-1124.

Horne, R.N.: "Reservoir Engineering of Reinjection," Course Notes. Stanford University, 1996.

Johri, M., Zoback, M.D., and Hennings, P.: "Observations of fault damage zones at reservoir depths," *Proceedings*, 45th US Rock Mechanics / Geomechanics Symposium, American Rock Mechanics Association. 2012.

Jourde, H., Flodin, E.A., Aydin, A., Durlofsky, L.J., Wen, X.H.: "Computing permeability of fault zones in eolian sandstone from outcrop measurements," *American Association of Petroleum Geologists Bulletin*, 86(7). 2002, 1187-1200.

Kreft, A., and Zuber, A.: "On the physical meaning of the dispersion equation and its solutions for different initial and boundary conditions," *Chemical Engineering Science*, 33(11). 1978, 1471-1480.

Lauwerier, H.A.: "The Transport of Heat in an Oil Layer Caused by the Injection of Hot Fluid," *Applied Scientific Research*, 5(2-3). 1955, 145-150.

Massart, B., Paillet, M., Henrion, V., Sausse, J., Dezayes, C., Genter, A., Bisset, A.: "Fracture characterization and stochastic modeling of the granitic basement in the HDR Soultz Project (France)," *Proceedings,* World Geothermal Congress. 2010.

Matsunaga, I., Yanagisawa, N., Sugita, H., and Tao, H.: "Reservoir monitoring by tracer testing during a long term circulation test at the Hijiori HDR site," *Proceedings*, Twenty-Seventh Workshop on Geothermal Reservoir Engineering, Stanford University, 2002.

Matsunaga, I., Yanagisawa, N., Sugita, H., Tao, H.: "Tracer tests for evaluation of flow in a multi-well and dual fracture system at the Hijiori HDR test site," *Proceedings*, World Geothermal Congress, 2005.

Maturgo, O.O., Sanchez, D. R., and Barroca, G.B.: "Tracer test using naphthalene disulfonates in Southern Negros Geothermal Production Field, Philippines," *Proceedings*, World Geothermal Congress, 2010.

Paul, P., Zoback, M.D., and Hennings, P.: "Fluid flow in a fracture reservoir using a geomechanically constrained fault-zone-damage model for reservoir simulation," *Proceedings*, 2007 SPE Annual Technical Conference and Exhibition.

Paul, P., Zoback, M.D., and Hennings, P.: "A method to implement permeability anisotropy associated with fault damage zones in reservoir simulation," *SPE Reservoir Evaluation and Engineering*, 14(1). 2011, 138-152.

Rivera, J.R., Ramirez, J.S., and Rodriguez, F.G.: "Parallel fractures model for tracer flow through geothermal reservoirs – preliminary results," *Proceedings*, 12th workshop on Geothermal Reservoir Engineering, Stanford University. 1987.